RESEARCH ARTICLE

IMMUNOLOGY

The epigenetic control of stemness in CD8$^+$ T cell fate commitment

Luigia Pace,[1,2,3]*† Christel Goudot,[1,2] Elina Zueva,[1,2] Paul Gueguen,[1,2] Nina Burgdorf,[1,2] Joshua J. Waterfall,[1,4,5] Jean-Pierre Quivy,[1,6,7] Geneviève Almouzni,[1,6,7]* Sebastian Amigorena[1,2]*

After priming, naïve CD8$^+$ T lymphocytes establish specific heritable transcription programs that define progression to long-lasting memory cells or to short-lived effector cells. Although lineage specification is critical for protection, it remains unclear how chromatin dynamics contributes to the control of gene expression programs. We explored the role of gene silencing by the histone methyltransferase Suv39h1. In murine CD8$^+$ T cells activated after *Listeria monocytogenes* infection, Suv39h1-dependent trimethylation of histone H3 lysine 9 controls the expression of a set of stem cell–related memory genes. Single-cell RNA sequencing revealed a defect in silencing of stem/memory genes selectively in *Suv39h1*-defective T cell effectors. As a result, *Suv39h1*-defective CD8$^+$ T cells show sustained survival and increased long-term memory reprogramming capacity. Thus, Suv39h1 plays a critical role in marking chromatin to silence stem/memory genes during CD8$^+$ T effector terminal differentiation.

Memory T lymphocytes provide lifelong protection against pathogens and cancer (*1*). In contrast to naïve and effector T cells, memory cells possess unique properties of "stemness," enabling long-term survival and plasticity to replenish effector pools after renewed antigen challenges (*2*). Understanding the lineage relationships among naïve, effector, and memory T cells, as well as the molecular pathways that regulate gene expression during the transitions from one to another of these distinct states, is essential for the rational design of vaccines and the development of new immune-therapeutic protocols (*3*).

Although many studies have characterized the transcription factors that control the differentiation of T cells, the corresponding epigenetic states and associated chromatin dynamics involved in the establishment and maintenance of CD8$^+$ T cell memory and effector identities is still incompletely understood (*4*–*7*). Several epigenetic pathways, including trimethylated histone H3 Lys^9 (H3K9me3)/HP-1/Suv39h1 and Polycomb repressive complexes, can contribute to establishing or maintaining transcriptional silencing (*7*–*11*). The H3K9me3 modification is considered to be a repressive mark, a hallmark of both constitutive and facultative heterochromatin (*12*), most often associated with silent gene loci. Mouse Suv39h1 and Suv39h2, two H3K9 site-specific histone methyltransferases (HMTs), are critical heterochromatin regulators (*10*, *13*). Suv39h1 is involved in heterochromatin organization, gene silencing, and lineage stability (*10*, *11*, *14*). It also limits somatic reprogramming of differentiated cells into induced pluripotent stem cells (*15*). In B cells and CD4$^+$ T cells, Suv39h1 is involved in gene silencing and lineage plasticity (*16*, *17*). Although the mechanisms underlying the induction of genes critically involved in effector and memory T cell generation have been extensively analyzed, the impact of heterochromatin-dependent gene expression silencing on the fates of T lymphocytes during differentiation has not been addressed. Here, we explore the role of Suv39h1-dependent gene silencing in the establishment and maintenance of memory CD8$^+$ T cell stemness, plasticity, and transition to terminally differentiated effectors.

Long-term protection against *Listeria monocytogenes* infection requires Suv39h1

To investigate the role of Suv39h1 in T cell responses to infectious agents, we infected *Suv39h1*-knockout (KO) and wild-type littermate mice with OVA-expressing *L. monocytogenes* (LM-OVA) (Fig. 1A). The bacterial burden in the spleen and liver was measured on day 3 (peak of infection in the spleen) and day 7 (resolution). After primary infection, we observed similar bacteremia in the spleen and liver of *Suv39h1*-KO and littermate control mice, both at the peak and after the resolution of infection (Fig. 1B). In contrast, upon a secondary challenge with LM-OVA 48 days after the primary infection, most littermate control mice showed complete protection, whereas high levels of LM-OVA were detected in the liver and/or spleen in more than 85% of *Suv39h1*-KO mice (Fig. 1C). Because protection against secondary *L. monocytogenes* infection is primarily mediated by CD8$^+$ T cells (*18*), these results suggested a defect in the CD8$^+$ T cell response against *L. monocytogenes* in *Suv39h1*-KO mice.

To further investigate the role of Suv39h1 in antigen-specific CD8$^+$ T cell responses to LM-OVA, we measured the antigen-specific CD8$^+$ T cell response using SIINFEKL (Ser-Ile-Ile-Asn-Phe-Glu-Lys-Leu)–H-2K^b multimers (K^b-OVA; Fig. 1D). We observed a factor of 2 reduction in the percentage and absolute numbers of K^b-OVA$^+$ CD8$^+$ T cells in the blood (Fig. 1, D and E) and a factor of 9 decrease in the numbers of K^b-OVA$^+$ CD8$^+$ T cells in the spleen (Fig. 1F) on day 7 in *Suv39h1*-KO mice relative to littermates. An analysis of K^b-OVA$^+$ CD8$^+$ T cells on days 5, 6, and 7 after LM-OVA infection suggests that the reduced antigen-specific response was not due to differences in the survival of *Suv39h1*-KO cells (fig. S1). Upon ex vivo restimulation, the percentages of interferon-γ$^+$ (IFN-γ$^+$) and granzyme B$^+$ CD8$^+$ T cells in *Suv39h1*-KO mice were lower than those of littermates (Fig. 1, D, G, and H, and fig. S2). To address whether the reduced K^b-OVA$^+$ CD8$^+$ T cell numbers in LM-OVA–infected *Suv39h1*-KO mice was T cell–intrinsic, we adoptively transferred *Suv39h1*-proficient or -deficient T cell receptor transgenic OT-I CD8$^+$ T cells (which recognize OVA) to wild-type mice. Five days after infection with LM-OVA, the numbers of *Suv39h1*-KO OT-I cells were reduced relative to wild-type OT-I (Fig. 1I). Although the percentage of IFN-γ$^+$ OT-I cells was similar, we observed a lower frequency of granzyme B$^+$ T cells (fig. S3, A to C), confirming that the defect observed in *Suv39h1*-KO mice was intrinsic to CD8$^+$ T cells. In line with these in vivo results, lower numbers of *Suv39h1*-KO effector OT-I CD8$^+$ T cells were recovered in vitro under effector-polarizing conditions, relative to numbers of *Suv39h1*-proficient T cells. Notably, the defective expansion in *Suv39h1*-KO T cells was overcome by the overexpression of SUV39H1 by a retroviral expression vector (fig. S4, A and B). Thus, CD8$^+$ T cell responses to LM-OVA are impaired in *Suv39h1*-KO mice because of a CD8$^+$ T cell–intrinsic defect.

Transcriptional silencing by Suv39h1

To investigate whether the reduced K^b-OVA$^+$ CD8$^+$ T cell response results from defective gene expression programming, we analyzed RNA profiles by Affymetrix microarrays of purified naïve and K^b-OVA$^+$ CD8$^+$ T cells, which were wild-type or *Suv39h1*-KO and isolated by fluorescence-activated cell sorting (FACS) 7 days after LM-OVA infection (Fig. 2A and fig. S5A). The overall number of transcripts up-regulated in K^b-OVA$^+$ CD8$^+$ T cells from infected mice, as compared to naïve CD8$^+$ T cells, was highly similar between littermates (1571) and *Suv39h1*-KO (1433) T cells (Fig. 2, B and C). In contrast, the number of transcripts

[1]Institut Curie, PSL Research University, F-75005 Paris, France. [2]INSERM U932, Equipes Labellisées Ligue contre le Cancer, F-75005 Paris, France. [3]Armenise-Harvard Laboratory, Italian Institute for Genomic Medicine, Turin, Italy. [4]INSERM U830, F-75005 Paris, France. [5]Institut Curie, Translational Research Department, F-75005 Paris, France. [6]CNRS, UMR3664, Equipe Labellisée Ligue contre le Cancer, F-75005 Paris, France. [7]Sorbonne Universités, UPMC University Paris 06, CNRS, UMR3664, F-75005 Paris, France. ***Corresponding author. Email: luigia.pace@iigm.it (L.P.); genevieve.almouzni@curie.fr (G.A.); sebastian.amigorena@curie.fr (S.A.)** †Present address: Italian Institute for Genomic Medicine, Turin, Italy.

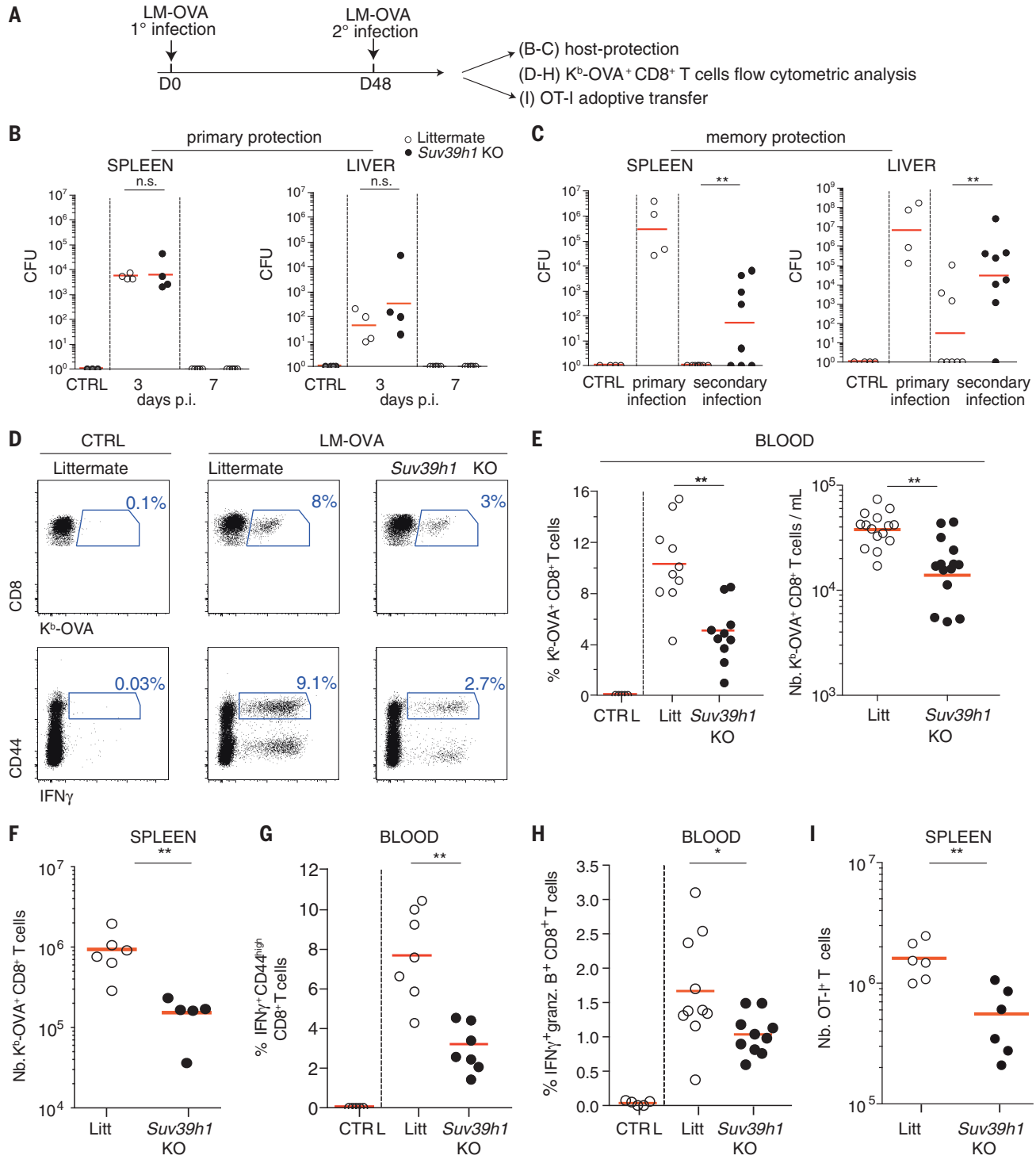

Fig. 1. CD8$^+$ T cell–mediated host protection is impaired in *Suv39h1*-defective mice. (**A**) Experimental design. (**B**) Littermates and *Suv39h1*-KO mice were intravenously (i.v.) injected with LM-OVA (primary infection) and, on the indicated days post-infection (p.i.), the number of bacterial colony-forming units (CFU) was determined. (**C**) Littermates and *Suv39h1*-KO mice previously i.v. immunized with LM-OVA were rechallenged 48 days later. Three days after LM-OVA secondary infection, protection was assessed by counting CFU in spleen and liver. (**D**) Littermate and *Suv39h1*-KO mice were immunized with LM-OVA; 7 days later, primary CD8$^+$ T cell responses were evaluated in the peripheral blood, using K^b-SIINFEKL (K^b-OVA$^+$) multimers and intracellular IFN-γ after restimulation ex vivo with the OVA peptide SIINFEKL (OVA$_{257\text{-}264}$). Representative plots are shown. (**E** and **F**) Percentages and numbers of K^b-OVA$^+$ CD8$^+$ T cells in the blood (E) and spleen (F). Data are representative of at least three experiments with two or more mice per group. (**G** and **H**) Percentages of CD44^{hi} IFN-γ$^+$ and IFN-γ$^+$ granzyme B$^+$, respectively, on gated CD8$^+$ T cells. (**I**) *Rag2*-KO mice were immunized with LM-OVA and adoptively transferred with wild-type and *Suv39h1*-KO OT-I cells. Five days later, the total number of OT-I cells was measured. Graphs show means; geometric means are displayed in (B), (C), (E) (right), (F), and (I). *P < 0.05, **P < 0.01 (Wilcoxon Mann-Whitney test); n.s., not significant.

significantly down-regulated in *Suv39h1*-KO mice (1108) was lower relative to littermates (1738) (Fig. 2, B and C). The absence of Suv39h1 expression impaired the transcriptional silencing of approximately 997 genes (Fig. 2C), including genes involved in critical T cell functions such as *Il7r* (CD127), *Sell* (CD62L), *Ccr7*, and *Cxcr4* (Fig. 2D) (*19*), consistent with the known repressive role of Suv39h1 in gene expression.

To examine the phenotype of the antigen-specific $CD8^+$ T cells that accumulate in *Suv39h1*-KO mice, we used gene set enrichment analysis (GSEA) by pairwise comparison between differentiated *Suv39h1*-KO and wild-type K^b-OVA^+ $CD8^+$ T cells isolated 7 days after LM-OVA infection (Fig. 2E). *Suv39h1*-KO cells showed significant enrichment in both memory and naïve gene signatures, whereas the effector signature was not significantly enriched in either wild-type or *Suv39h1*-KO K^b-OVA^+ $CD8^+$ T cells (Fig. 2E). The interrogation of a series of public gene signatures revealed that *Suv39h1*-KO K^b-OVA^+ $CD8^+$ T cells were also significantly enriched for a "lymphoid–stem cell" signature (*20*) (Fig. 2E, right). For further investigation of the nature of these differences, the core lymphoid–stem cell gene signature (*20*) was combined with gene sets known

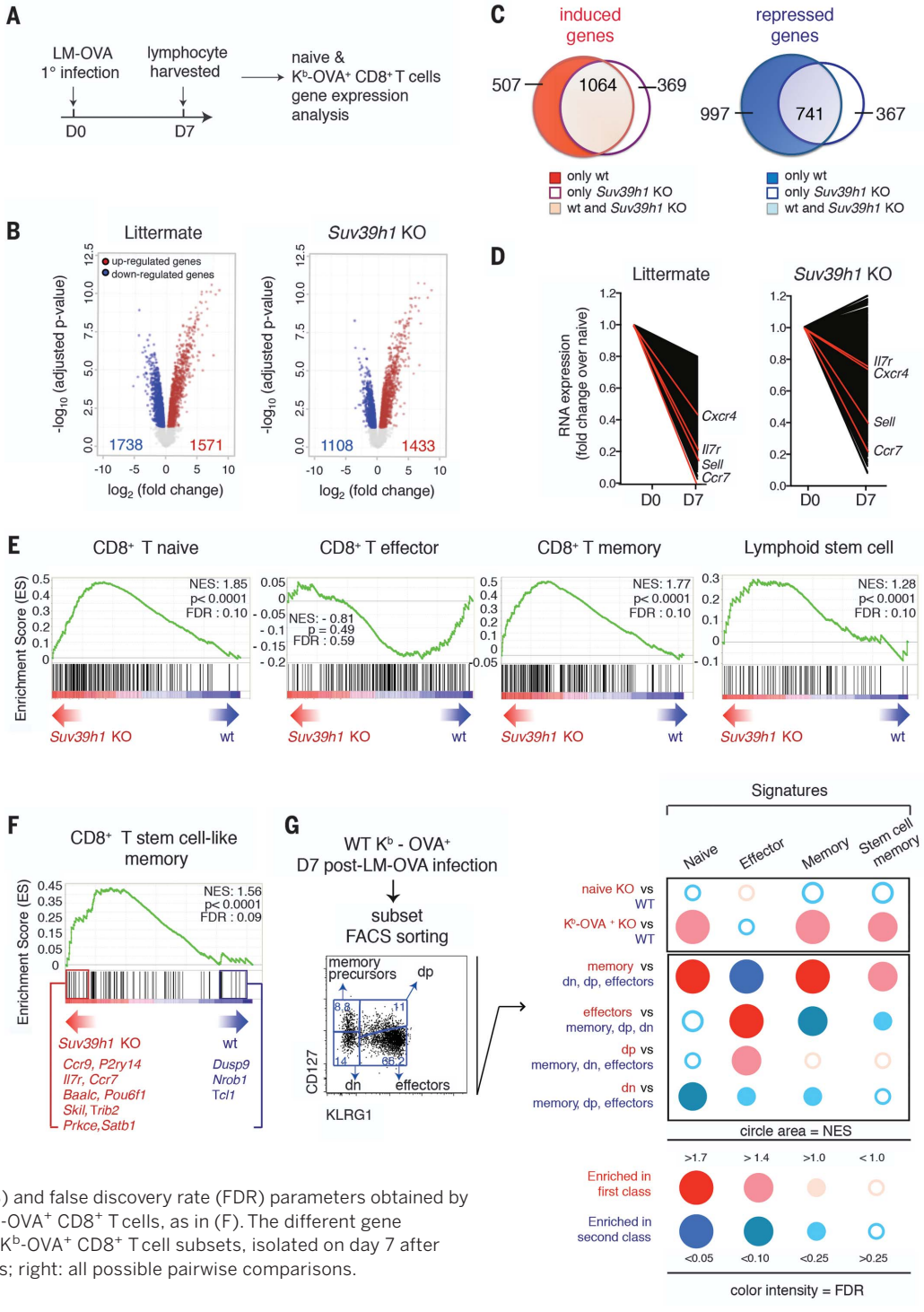

Fig. 2. Gene expression patterns and differentiation programs of K^b-OVA^+ $CD8^+$ T lymphocytes are enriched in stem cell–like gene signatures in *Suv39h1*-KO mice. (**A**) Experimental design. Naïve littermate and *Suv39h1*-KO $CD8^+$ T cells and day 7 p.i. K^b-OVA^+ $CD8^+$ T cells (from LM-OVA–infected mice) were isolated by FACS. RNA was isolated and analyzed using Affymetrix microarrays (three mice per condition were analyzed). (**B**) Volcano plots of K^b-OVA^+ $CD8^+$ T cells versus naïve $CD8^+$ T cells from littermate and *Suv39h1*-KO mice show the adjusted *P* value ($-\log_{10}$) versus fold change ($\log_2$). Up-regulated and down-regulated mRNAs are shown in red and blue, respectively. (**C**) Venn diagrams summarize the overlap between differentially expressed genes that are up-regulated (left) or down-regulated (right) in K^b-OVA^+ $CD8^+$ T cells versus naïve $CD8^+$ T cells from wild-type and *Suv39h1*-KO mice. Total common gene numbers for each group are indicated within the areas. (**D**) Expression pattern of mRNAs down-regulated in wild-type K^b-OVA^+ $CD8^+$ T cells versus naïve cells, shown for wild-type and *Suv39h1*-KO $CD8^+$ T cells. Representative genes are shown with red lines. (**E**) GSEA was performed to determine the specific enrichment in gene signatures (GeneSet) in wild-type and *Suv39h1*-KO K^b-OVA^+ $CD8^+$ T cells isolated on day 7 after LM-OVA infection. (**F**) GSEA for stem/memory signature (table S1) in wild-type and *Suv39h1*-KO K^b-OVA^+ $CD8^+$ T cells. The top highly expressed mRNAs in *Suv39h1*-KO or in wild-type K^b-OVA^+ $CD8^+$ T cells are shown. (**G**) BubbleGUM analysis of homologies between different $CD8^+$ T subsets by high-throughput GSEA. The right panel summarizes the normalized enrichment score (NES) and false discovery rate (FDR) parameters obtained by GSEA of wild-type and *Suv39h1*-KO K^b-OVA^+ $CD8^+$ T cells, as in (F). The different gene signatures were analyzed in wild-type K^b-OVA^+ $CD8^+$ T cell subsets, isolated on day 7 after LM-OVA infection. Left: Sorted subsets; right: all possible pairwise comparisons.

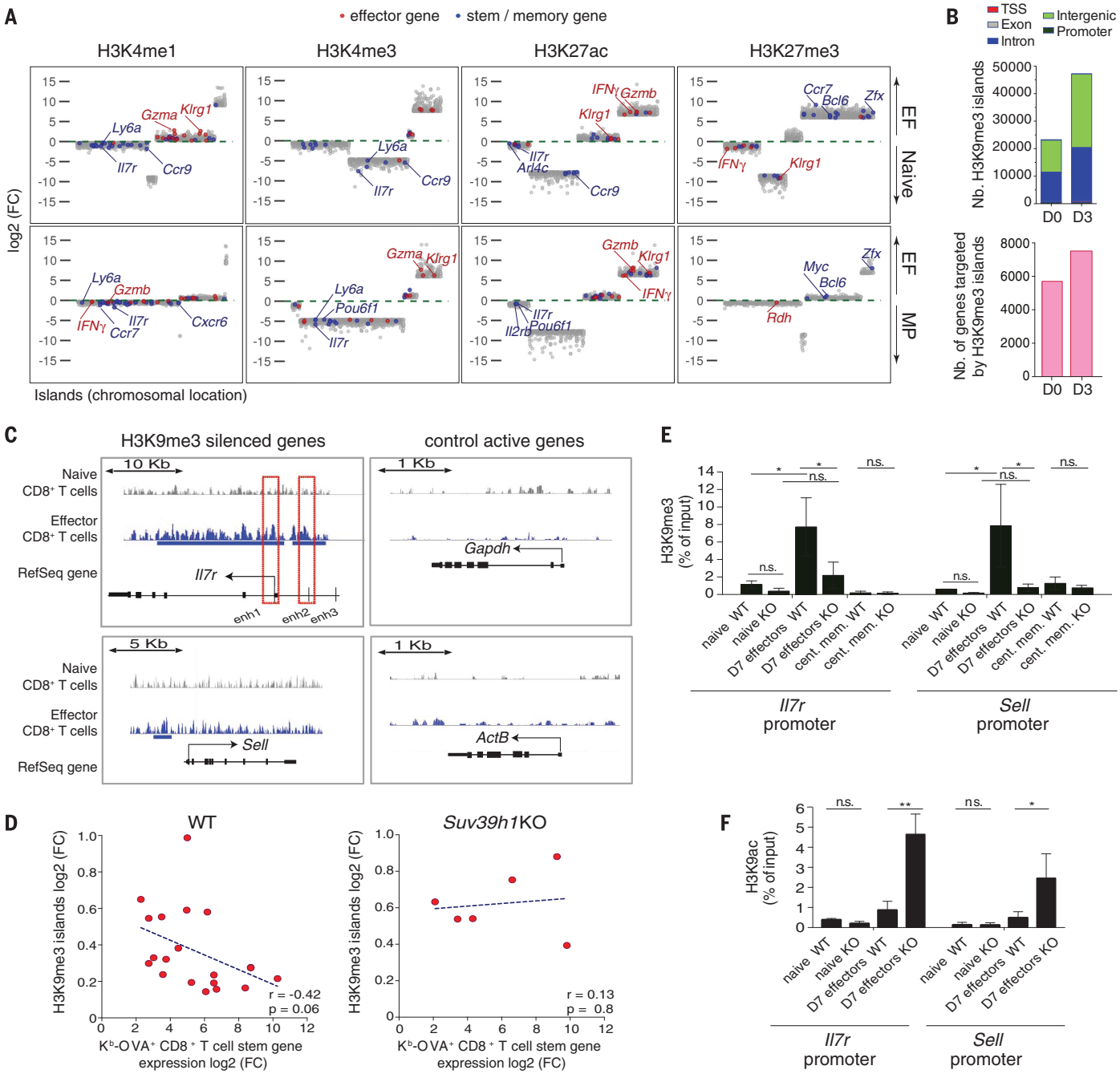

Fig. 3. H3K9me3 deposition by Suv39h1 silences stem cell–like memory genes during CD8$^+$ T effector differentiation. (**A**) H3K4me1, H3K4me3, H3K27ac, and H3K27me3 fold change (FC) values in enriched domains (islands) from naïve cells or memory precursors were compared to effector OT-I CD8$^+$ T cells (differentiated in vivo 8 days after LM-OVA infection) to identify significant differentially modified regions. Islands assigned to stem/memory and effector genes are shown in blue and red, respectively. (**B** and **C**) Naïve and in vitro cultured wild-type CD8$^+$ T effectors were analyzed by ChIP-seq using antibodies to H3K9me3. (B) Top: The genomic distribution of H3K9me3-enriched islands is increased in effectors. Bottom: The number of genes targeted by H3K9me3-enriched islands is also increased. Means of two biological replicates are shown. (C) Representative genomic regions show H3K9me3 enrichment in naïve and effector CD8$^+$ T cells. Normalized ChIP-seq reads (bigWig) and enriched islands (bed) are shown. In the left panels, *Il7r* and *Sell* inter- and intragenic regions with normalized ChIP-seq reads and significantly H3K9me3 enriched islands are represented. Transcribed control genes are also shown in the right panels. (**D**) H3K9me3 enrichment is plotted against mRNA expression of stem cell/memory signature genes. H3K9me3 island deposition in in vitro differentiated effectors correlates with stem/memory gene silencing in wild-type dump$^-$ K^b-OVA$^+$ CD8$^+$ T cells and is impaired in *Suv39h1*-KO effectors. Pearson linear regression is displayed. (**E**) Littermate and *Suv39h1*-KO polyclonal naïve (CD44^{lo} CD62L$^+$ CD127$^+$) CD8$^+$ T cells, central memory (CD44^{hi} CD62L$^+$ CD127$^+$) CD8$^+$ T cells, and effector (dump$^-$ CD44^{hi} CD127$^{lo/-}$ KLRG1$^+$ K^b-OVA$^+$) CD8$^+$ T cells isolated 7 days after LM-OVA infection were analyzed by μChIP-qPCR using antibodies to H3K9me3. qPCR was performed with primers specific for the promoters of *Il7r* and *Sell*. (**F**) Naïve and effector (dump$^-$ CD44^{hi} CD127$^{lo/-}$ KLRG1$^+$ K^b-OVA$^+$) CD8$^+$ T cells from day 7 LM-OVA infected mice were analyzed by μChIP-qPCR using antibodies to H3K9ac. Data are means ± SEM of at least three independent experiments. *P < 0.05, **P < 0.01; for (E) and (F), analysis of variance, Tukey test.

to be commonly enriched both in memory CD8$^+$ T cells and long-term hematopoietic stem cells (*21*), overexpressed in mouse and human CD8$^+$ T stem cell–like memory subset (*22*) and also retrieved from signaling pathways that regulate stem cell pluripotency from the KEGG database. We designated this as a "stem cell–like memory" signature (composed of 86 genes; table S1). K^b-OVA$^+$ CD8$^+$ T cells from LM-OVA–infected *Suv39h1*-KO mice were strongly enriched for this signature (Fig. 2F and fig. S5, B and C). The expression levels of stem cell–like and memory markers *Il7r*, *Ly6a* (Ly6a/e, Sca-1), *Fas* (CD95), and *Pou6f1* were all increased in *Suv39h1*-KO K^b-OVA$^+$ CD8$^+$ cells relative to cells from control littermates (table S1 and fig. S5C). The CD8$^+$ T–stem cell–like memory signature was not enriched in naïve *Suv39h1*-KO CD8$^+$ T cells relative to wild-type littermates (Fig. 2G, BubbleGUM representation, top) (*23*). Thus, by comparison to wild-type cells, *Suv39h1*-KO K^b-OVA$^+$ CD8$^+$ T cells overexpress a series of genes associated with stem cells and memory functions.

To search for these stem cell/memory CD8$^+$ T cells in wild-type animals, we isolated the following wild-type subpopulations by FACS (from dump$^-$ CD44^{hi} K^b-OVA$^+$ CD8$^+$ T cells, day 7 after LM-OVA infection): (i) CD127^{hi} KLRG1$^-$ memory precursors, (ii) CD127$^{lo/-}$ KLRG1$^+$ effectors, (iii) CD127$^+$ KLRG1$^+$ double-positive cells, and (iv) CD127$^-$ KLRG1$^-$ double-negative cells (Fig. 2G, left), as described previously (*5*, *19*). The RNA expression profile of these four FACS-sorted populations was analyzed using Affymetrix microarrays. We tested each of the four subsets (test class) against a combination of the three other FACS-sorted subpopulations, using high-throughput GSEA for the CD8$^+$ T naïve, memory, effector, and stem cell–like/memory signatures (Fig. 2G, lower right). As expected, sorted memory precursors were enriched for both memory and naïve signatures, whereas sorted effectors were enriched for the effector signature (Fig. 2G, right). Notably, only sorted memory precursors from wild-type mice were enriched for the CD8$^+$ T stem cell–like signature when compared to the three other sorted subpopulations (Fig. 2G, lower right). Thus, the stem cell–like memory signature, which is specific to memory precursors in wild-type T cells, is broadly enriched in bulk K^b-OVA$^+$ CD8$^+$ T cells in *Suv39h1*-KO mice.

H3K9me3 deposition at stem/memory-associated loci

To elucidate the epigenetic states (*11*) associated with the stem/memory and effector (*19*, *21*) gene loci (tables S1 and S2), we first analyzed a set of public chromatin immunoprecipitation sequencing (ChIP-seq) data sets, generated with naïve, memory precursor, and effector OT-I CD8$^+$ T cells isolated 8 days after LM-OVA infection in vivo (*24*). We identified the regions significantly enriched for monomethylated histone H3 Lys^4 (H3K4me1), trimethylated histone H3 Lys^4 (H3K4me3), acetylated histone H3 Lys^{27} (H3K27ac), and trimethylated histone H3 Lys^{27} (H3K27me3) histone marks. For each histone mark, the significantly enriched islands were associated with the nearest gene (*25*). Differences in histone mark relative enrichment were calculated by pairwise comparison of terminal effectors to naïve cells (Fig. 3A, top) or to memory precursors (Fig. 3A, bottom). The regions associated with the stem cell–like memory genes showed an enrichment in H3K4me1 and H3K4me3 in both naïve cells and memory precursors, as compared to terminal effectors. The enrichment in these active marks, H3K4me1 and H3K4me3, corresponds to the transcription level of the stem cell–like memory genes in both wild-type naïve and memory precursors, as compared to effectors (fig. S5B). In contrast, the profile of H3K27ac deposition, typically distal, was more difficult to associate with target genes, including certain stem/memory genes and most effector signature genes in effectors (Fig. 3A); of note, cell cycle genes were excluded from this signature (table S2). In line with these results, H3K4me1 and H3K27ac marked the effector genes mostly in the effector subset (Fig. 3A). The enrichment of the repressive mark H3K27me3 on stem cell–like memory genes corresponded with the silencing of the gene signature in the effector CD8$^+$ T cells (Fig. 3A and fig. S5B). Thus, post-translational chromatin modifications corresponding to transcriptionally active and repressive marks follow the stem cell–like memory and effector gene expression patterns defined in memory precursors and effector T cell populations, respectively.

To investigate the contribution of Suv39h1-dependent chromatin changes, we performed ChIP-seq for the repressive mark H3K9me3 in naïve and in vitro differentiated effector CD8$^+$ T cells from wild-type and *Suv39h1*-KO mice (fig. S6A). The total numbers of H3K9me3 islands and targeted genes were higher in wild-type effectors than in wild-type naïve CD8$^+$ T cells (Fig. 3B and fig. S6B). Most de novo H3K9me3 islands (present in effector but not in naïve T cells) were distal to the transcription start site (TSS), with equal proportions of intra- and intergenic locations (Fig. 3B, top), and with highest enrichment between 10 and 100 kb from the TSS (fig. S6C). Thus, H3K9me3 is broadly distributed in both wild-type naïve and effector CD8$^+$ T cells, and the number of H3K9me3 islands increases in effector CD8$^+$ T cells relative to naïve CD8$^+$ T cells.

Among the 997 genes that are less efficiently silenced in vivo in *Suv39h1*-KO cells relative to littermates (Fig. 2C), 145 genes were decorated by H3K9me3 (fig. S6C). Several of these genes encode immune and stem/memory-related proteins, including CD127 or CD62L (Fig. 3C). In effectors, the *Il7r* gene acquires H3K9me3 at sites both proximal and distal to the TSS, including the promoter, previously described enhancers, introns, and intergenic regions (Fig. 3C, upper left) (*26*). H3K9me3 deposition is also increased at the *Sell* locus, upstream the promoter region, in effectors as compared to naïve CD8$^+$ T cells (Fig. 3C, lower left). No significantly enriched H3K9me3 islands were found for actively transcribed housekeeping and control genes (Fig. 3C, right). These results suggest that H3K9me3 silences genes linked to naïve versus effector differentiation, including *Il7r* and *Sell*.

To evaluate whether these stem cell–like memory gene loci are direct targets of Suv39h1, we compared the relative (fold change) enrichment of H3K9me3 islands detected in effectors to stem cell/memory gene expression in wild-type and *Suv39h1*-KO K^b-OVA$^+$ CD8$^+$ T cells (Fig. 3D). H3K9me3 enrichment negatively correlated with mRNA expression of stem cell/memory signature genes in wild-type but not in *Suv39h1*-KO K^b-OVA$^+$ CD8$^+$ T cells (Fig. 3D). In contrast, none of the H3K9me3 domains were associated with effector signature genes. Thus, the silencing of stem cell–like memory genes correlated with significant H3K9me3 enrichment in wild-type but not in *Suv39h1*-KO T cells, in which increased gene expression correlated with reduced or absent H3K9me3 deposition.

To validate and refine these results, we used μChIP–quantitative polymerase chain reaction (qPCR) analysis of H3K9me3 at critical gene loci in naïve (CD44^{lo} CD62L$^+$ CD127$^+$), central memory (CD44^{hi} CD62L$^+$ CD127$^+$), and effector (dump$^-$ CD44^{hi} CD127$^{lo/-}$ KLRG1$^+$ K^b-OVA$^+$) CD8$^+$ T cells purified 7 days after LM-OVA infection. Naïve cells showed barely detectable H3K9me3 at both the *Il7r* and *Sell* promoters (Fig. 3E and fig. S6D), whereas in effector T cells, the levels of H3K9me3 were increased at both loci, again in correlation with gene silencing (Fig. 3E). Consistent with the expression results, central memory cells, like naïve cells, have low levels of H3K9me3 at both promoters, whereas the reduced expression of *Il7r* and *Sell* in effector cells correlated with H3K9me3 enrichment.

Suv39h1-KO effector CD8$^+$ T cells did not show a significant increase of H3K9me3 at the *Il7r* or *Sell* loci, consistent with impaired silencing of *Il7r* and *Sell* expression (Figs. 2D and 3E). Likewise, CD8$^+$ central memory T cells and naïve cells presented low levels of H3K9me3 at both the *Sell* and *Il7r* promoters (Fig. 3E). Also consistent with these results, the level of the alternative active mark H3K9ac is increased in effectors at both *Il7r* and *Sell* loci in *Suv39h1*-KO CD8$^+$ T cells alone, which was again consistent with gene expression profiles (Fig. 3F). These results indicate that Suv39h1 dynamically decorates genes encoding important regulators of CD8$^+$ T cell stem/memory fate with H3K9me3, and that these genes are silenced in wild-type CD44^{hi} CD127$^{lo/-}$ KLRG1$^+$ K^b-OVA$^+$ CD8$^+$ T effectors. In *Suv39h1*-KO antigen-specific CD8$^+$ T cells, these stem/memory genes fail to acquire the repressive mark, resulting in defective silencing.

Long-lasting memory and short-lived effector CD8$^+$ T cell differentiation

These gene expression results suggest that the *Suv39h1* defect may affect memory versus effector differentiation in vivo. No major differences between wild-type and *Suv39h1*-KO were observed in terms of CD44, CD122, and PD1 expression patterns (fig. S7A) in blood K^b-OVA$^+$ CD8$^+$ T cells 7 days after LM-OVA infection. In contrast, CD127 expression was increased in both memory precursors (KLRG1$^-$) and effector cells (KLRG1$^+$) in *Suv39h1*-KO mice relative to

littermates (Fig. 4A). The increased proportion of CD127^{+} cells was due to decreased numbers of CD127$^{lo/-}$ KLRG1^{+} effector T cells (Fig. 4, A and B, right). The absolute numbers of CD127^{lo} cells (both KLRG1^{+} and KLRG1^{-}) were reduced, whereas the number of CD127^{high} memory precursor cells was unchanged (Fig. 4, A and B, left). In *Suv39h1*-KO mice, K^{b}-OVA^{+} CD8^{+} T cells also included a lower proportion of CD27^{lo} cells and impaired down-regulation of CD62L in a subpopulation of cells (fig. S7, A and B). Enhanced memory differentiation of wild-type/*Suv39h1*-KO 1:1 mixed bone marrow chimeras upon LM-OVA infection resulted in a significantly higher proportion of effectors among wild-type cells, whereas the proportion of memory precursors was increased among *Suv39h1*-KO K^{b}-OVA^{+} T cells (Fig. 4C and fig. S8). Similar results were obtained after the adoptive transfer of wild-type and *Suv39h1*-KO OT-I CD8^{+} T cells (fig. S3, D and E). Thus, *Suv39h1*-KO mice develop increased proportions of memory T cells in response to *L. monocytogenes* infection as the result of a T cell–intrinsic defect in effector differentiation.

We next sought to determine the impact of the *Suv39h1* defect on long-term memory versus

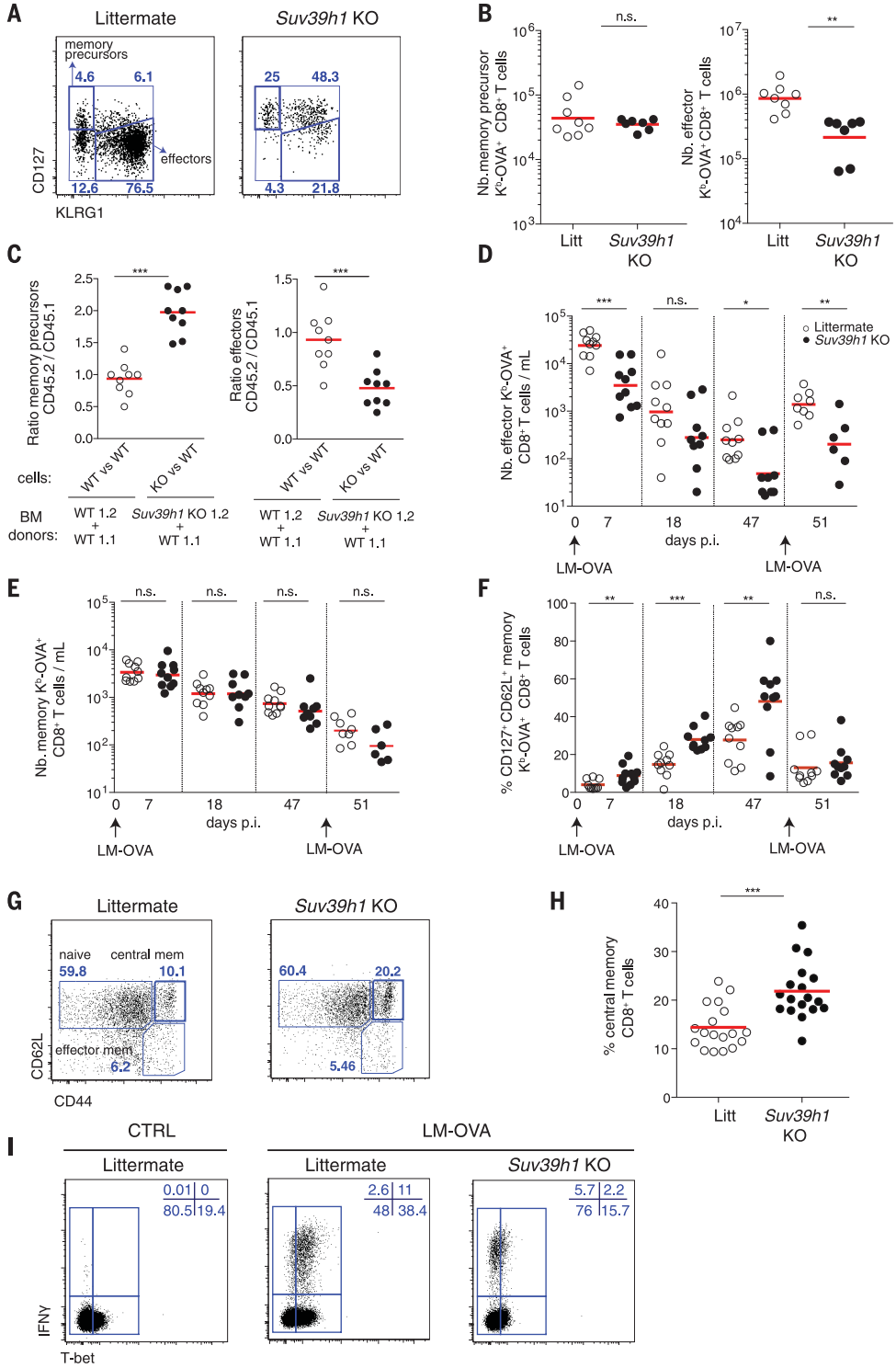

Fig. 4. Suv39h1 is a critical regulator of peripheral effector versus memory CD8^{+} T differentiation. (**A**) Littermate and *Suv39h1*-KO mice were infected with LM-OVA. Seven days later, dump^{-} CD44^{hi} K^{b}-OVA^{+} CD8^{+} T cells in the spleen were analyzed according to CD127 and KLRG1 staining (CD127^{hi} KLRG1^{-} memory precursors and CD127$^{lo/-}$ KLRG1^{+} differentiated effector cells). Representative dot plots are shown; numbers represent the percentages. (**B**) Numbers of memory precursors and effectors in the spleen were measured. (**C**) Wild-type and *Suv39h1*-KO mixed bone marrow chimeras were infected with LM-OVA, and 7 days later the ratio between memory precursors and short-lived effector CD8^{+} T cells was evaluated in peripheral blood using K^{b}-OVA^{+} multimers. (**D** to **F**) Mice were infected with LM-OVA on day 0 (primary infection) and day 48 (secondary infection). On days 7, 18, 47, and 51 p.i. (with respect to the primary infection), numbers of short-lived effectors (D) and central memory cells (E) on gated dump^{-} CD44^{hi} K^{b}-OVA^{+} CD8^{+} T cells per ml of peripheral blood were measured. (F) Longitudinal analysis of the dynamics of central memory K^{b}-OVA^{+} CD8^{+} T cells. (**G**) Representative dot plots of gated blood CD8^{+} T lymphocytes; numbers represent percentages. (**H**) Percentage of blood endogenous polyclonal central memory CD8^{+} T cells. (**I**) Peripheral blood cells from LM-OVA–infected littermate and *Suv39h1*-KO mice were stimulated ex vivo 7 days after infection with the OVA peptide SIINFEKL (OVA$_{257-264}$) and analyzed for intracellular T-bet expression and IFN-γ production. Representative dot plots are shown; numbers represent percentages. Data are shown as geometric means in (B), (D), and (E) or as means in (C), (F), and (H). *P < 0.05, **P < 0.01, ***P < 0.001 (Wilcoxon Mann-Whitney test).

effector differentiation and persistence. The numbers of K^b-OVA$^+$ CD8$^+$ T memory cells and effectors were analyzed 7, 18, and 47 days after LM-OVA infection, and 3 days after rechallenge on day 51. As expected from previous results (Fig. 4B), the number of effectors was reduced at all times, including at the peak of the rechallenge memory response in the blood (Fig. 4D) and spleen (fig. S9, right). The numbers of memory cells did not change between wild-type and *Suv39h1*-KO at the peak of the response, during contraction, or after rechallenge (Fig. 4E and fig. S9, left). The proportion of central memory (CD44^{hi} CD62L$^+$ CD127$^+$ K^b-OVA$^+$) CD8$^+$ T cells (*27*) increased over time in *Suv39h1*-KO mice as compared to wild-type mice (Fig. 4F). Notably, the percentage of endogenous subsets of memory CD8$^+$ T cells in *Suv39h1*-KO mice was also higher, including polyclonal CD62L$^+$ central memory CD8$^+$ T cells in the blood and secondary lymphoid organs (Fig. 4, G and H, and fig. S10, A to C), CD62L$^-$ effector memory CD8$^+$ T cells in the bone marrow and blood (fig. S10D), and tissue-resident CD8$^+$ T cells in the liver (fig. S10, F to H). The endogenous *Suv39h1*-KO central memory CD8$^+$ T cells also expressed increased levels of memory and stem cell–like memory markers SCA-1 and CD95 (fig. S10E) (*22*, *27*, *28*) Thus, *Suv39h1*-KO mice show higher levels of central and effector memory CD8$^+$ T cells both before and after LM-OVA challenge.

An analysis of master regulators involved in memory and effector differentiation showed that the proportion of LM-OVA–specific T cells expressing T-bet is reduced in both IFN-γ^+ and IFN-γ^- *Suv39h1*-KO cells as compared to littermates (Fig. 4I and fig. S11). Similarly, the expression of Eomes, Blimp1, and Bcl6 was also reduced (fig. S11). Thus, *Suv39h1*-KO CD8$^+$ T cells display a central memory–like phenotype but express reduced levels of both effector and memory transcription master regulators (*4*, *5*).

Previous adoptive transfer experiments showed that only CD127$^+$ memory precursors give rise to long-term memory cells and confer protective immunity (*29*). To evaluate their in vivo memory self-renewal and differentiation properties, we isolated wild-type and *Suv39h1*-KO CD45.2 K^b-OVA$^+$ CD8$^+$ T cells 7 days after LM-OVA infection and adoptively transferred them at low numbers into naïve congenic CD45.1 recipients (Fig. 5A and fig. S12A). Forty days after challenge with LM-OVA, as expected, few wild-type K^b-OVA$^+$ T cells persisted or responded to the LM-OVA challenge. In contrast, donor *Suv39h1*-KO CD45.2 K^b-OVA$^+$ T cells were clearly present and responded to the infection (Fig. 5, B and C), with an increased proportion of memory precursor and effector cells (Fig. 5, B and D, left). To further evaluate the self-renewal properties of wild-type and *Suv39h1*-KO central memory T cells, we isolated total CD45.2$^+$ CD44^{hi} CD62L$^+$ CD127$^+$ KLRG1$^-$ K^b-OVA$^-$ central memory T cells, harvested 7 days after LM-OVA infection, and transferred them into naïve CD45.1 congenic mice (Fig. 5A and fig. S12A). Thirty-nine days after adoptive transfer, similar numbers of wild-type and *Suv39h1*-KO donor CD8$^+$ T cells, which had maintained a central memory phenotype, were present in the blood (Fig. 5G, left, and fig. S12B). Four days after LM-OVA rechallenge, however, both the percentage and the total numbers of *Suv39h1*-KO donor CD8$^+$ T cells were increased relative to control *Suv39h1*-sufficient cells (Fig. 5, E and G, right). Donor *Suv39h1*-KO CD8$^+$ T cells displayed higher expression of both CD127 and CD62L, lower levels of KLRG1 and CD44, a slight decrease in the expression of SCA-1, and similar levels of CD122 (Fig. 5, E and F). The donor memory subset was increased in the animals adoptively transferred with *Suv39h1*-KO T cells (Fig. 5H). Thus, *Suv39h1*-KO K^b-OVA$^+$ and central memory CD8$^+$ T cells have superior self-renewal and repopulation potential relative to their wild-type counterparts.

Stemness gene silencing in terminal effectors requires Suv39h1

Increased proportions of T cells with a central memory phenotype and stem cell–like properties were found in *Suv39h1*-KO mice. This phenotype could be due to the accumulation of a defined population of stem cell–like memory T cells, or to the expression of stem cell–related genes across different T cell subpopulations. We used single-cell RNA sequencing (scRNA-seq) to explore and dissect the heterogeneity of wild-type and *Suv39h1*-KO K^b-OVA$^+$ CD8$^+$ T lymphocytes. Purified naïve and K^b-OVA$^+$ CD8$^+$ T cells from wild-type and *Suv39h1*-KO mice were isolated by FACS 7 days after LM-OVA infection and processed for scRNA-seq (fig. S13). For naïve cells, we sequenced 1102 and 991 cells from wild-type and *Suv39h1*-KO mice, respectively. For antigen-specific K^b-OVA$^+$ CD8$^+$ T cells, we processed two technical replicates for both wild-type and *Suv39h1*-KO infected mice (approximately 1200 and 1000 cells, respectively) and an additional biological replicate (from different mice, 404 wild-type and 283 *Suv39h1*-KO K^b-OVA$^+$ CD8$^+$ T cells). The cells from the two technical replicates were pooled and used for the rest of the analysis. A comparison between technical and biological replicates within wild-type and *Suv39h1*-KO mice showed a strong correlation (figs. S13 to S15).

A principal components analysis (PCA) of differentially expressed genes by wild-type and *Suv39h1*-KO naïve and K^b-OVA$^+$ CD8$^+$ T cells, is visualized as a set of *t*-distributed stochastic neighbor embedding (*t*-SNE) plots in Fig. 6A. In wild-type cells, unsupervised clustering of naïve and K^b-OVA$^+$ CD8$^+$ T cells revealed eight clusters in wild-type T cells and six clusters in *Suv39h1*-KO antigen-specific K^b-OVA$^+$ CD8$^+$ T cells (fig. S14, A and B, and tables 3 and 4). On the basis of distinct transcription profiles, we grouped the unsupervised clusters into four major subset categories: naïve, memory precursor, effector, and cycling cells (Fig. 6, B to D, and fig. S14C). As expected, the naïve cells grouped in a homogeneous category characterized by the highest expression of *Sell*, *Ccr7*, and *Tcf7* (Fig. 6B). The memory precursors were enriched in *Il7r*, *Cxcr3*, *Cd27*, *Cd28*, and *Ly6a* expression (Fig. 6, B and E); the effectors were characterized by *Zeb2*, *Klrg1*, and *granzyme B* (Fig. 6, B and E, and fig. S16); and the cycling subsets were defined by cell cycle genes including *Pcna* and *Mcm5* (Fig. 6, B and E, right). Although effectors represented the majority of multimer-positive CD8$^+$ T cells when analyzed by FACS (CD127$^-$ KLRG1$^+$), the terminally differentiated effectors only represented approximately 30% of K^b-OVA$^+$ CD8$^+$ T cells in the categories defined by scRNA-seq (Fig. 6D). This is likely due to the resolution of the cycling cells, which also express high levels of different effector markers, including KLRG1 and granzyme A and B (Fig. 6, B and E, and fig. S16). Consistent with flow cytometric analysis, the proportion of *Suv39h1*-KO effector K^b-OVA$^+$ CD8$^+$ T cells was decreased (Fig. 6D and fig. S14). Thus, unsupervised scRNA-seq allows resolution of the expected memory precursors and effector populations among K^b-OVA$^+$ CD8$^+$ T cells. The scRNA-seq analysis also reveals a population expressing high levels of genes involved in the cell cycle, as well as markers of memory precursors and effectors.

Having defined the different populations of antigen-specific CD8$^+$ T cells, we next sought to analyze the expression of stem cell/memory genes in wild-type and *Suv39h1*-KO cells. As expected, wild-type cells showed enrichment of stem cell markers (i.e., *Cxcr6*, *Rnf138*, *Il18r1*, and *Traf1*) in the memory precursors (Fig. 6F). In *Suv39h1*-KO T cells, the expression of these markers was also high in memory precursors, but, in contrast to wild-type cells, expression was also detected in effector and cycling populations. Similar increased expression of the stem/memory signature in *Suv39h1*-KO effectors could be visualized on *t*-SNE plots where the number of genes from the stem/memory signature per cell is represented by a color scale (Fig. 6G). These results suggest that *Suv39h1*-defective effectors express higher levels of certain stem/memory-related genes, consistent with impaired silencing.

To further analyze the expression of the stem cell–like memory and effector signature genes at the single-cell level among the different populations, we used density scatterplots in which the numbers of genes from each signature are represented against each other (Fig. 6H). In most naïve cells from both wild-type and *Suv39h1*-KO mice, we detected an average of seven stem/memory signature genes per cell, and fewer than four genes from the effector signature. As expected, in the wild type, memory precursors, relative to naïve cells, expressed higher numbers of genes from the stem/memory signature (mean of 9 genes per cell; 43% with more than 10 genes per cell) as well as high numbers of genes from the effector signature (mean of 18 genes per cell). The proportion of effector cells expressing high numbers (>10 per cell) of stem/memory genes was reduced (16%) as compared with memory cells (43%), whereas there was only a modest increase in the number of genes from the effector signature (mean 20 genes). Of note, the gene expression levels from the effector signature were strongly increased in effectors as compared to memory cells (Fig. 6B and fig. S16). Notably, cycling cells coexpressed either low or high numbers of

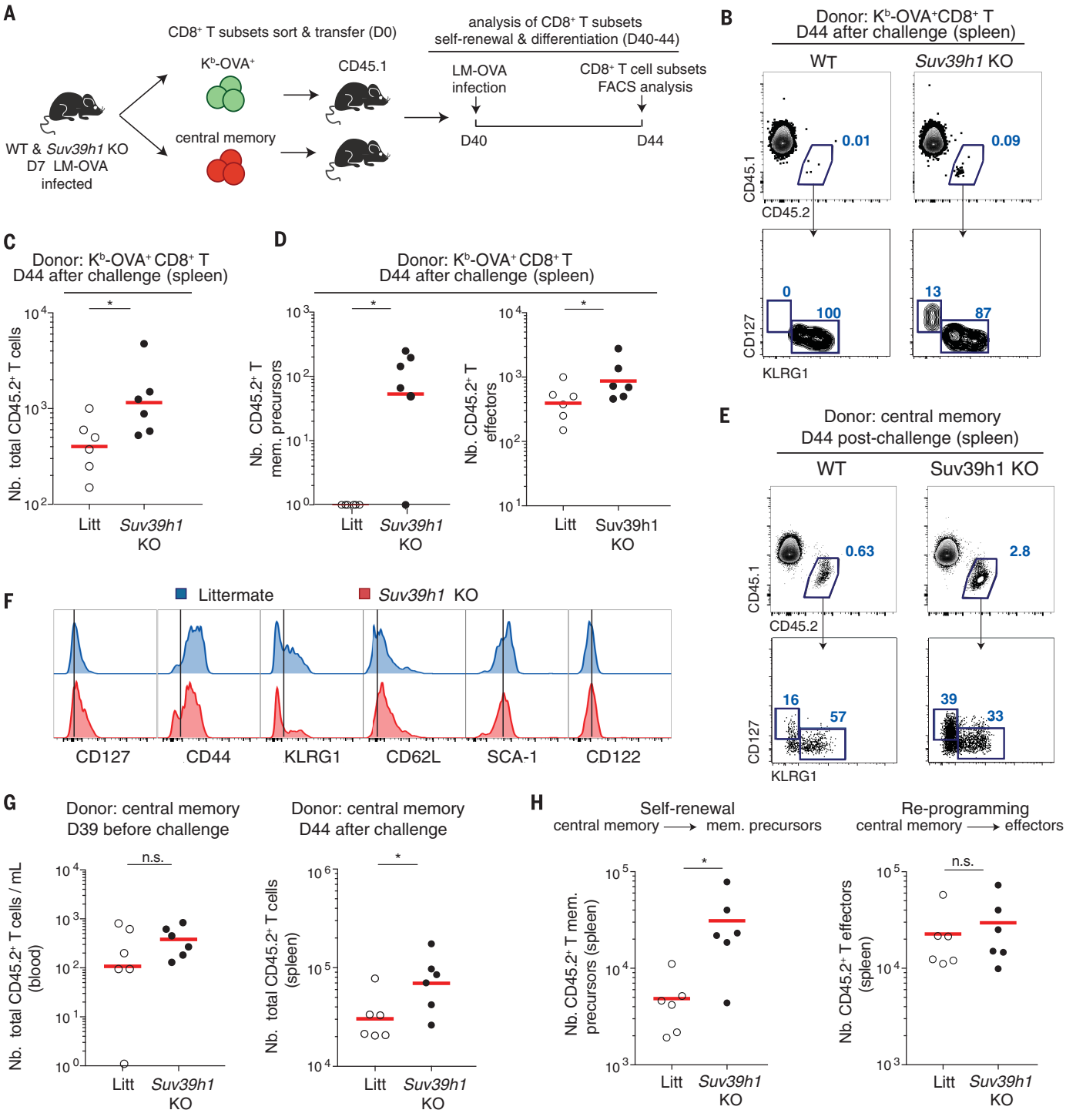

Fig. 5. Suv39h1-mediated defective silencing during CD8$^+$ T cell lineage commitment results in the accumulation of stem cell–like central memory cells. (**A**) Experimental design. Dump$^-$ K^b-OVA$^+$ CD8$^+$ T cells or CD44^{hi} CD62L$^+$ CD127$^+$ K^b-OVA$^-$ central memory CD8$^+$ T cells, isolated 7 days after LM-OVA infection from littermate or *Suv39h1*-KO mice, were adoptively transferred to naïve congenic CD45.1$^+$ recipient mice. The recipients were challenged with LM-OVA 40 days later. (**B**) Donor CD45.2$^+$ K^b-OVA$^+$ CD8$^+$ T cells were analyzed in the spleen 4 days after infection. Representative dot plots and a phenotypic analysis of subsets are shown; numbers represent percentages. (**C**) Numbers of total donor CD45.2$^+$ CD8$^+$ T cells. (**D**) Numbers of donor CD127$^+$ KLRG1$^-$ memory precursors and CD127$^{lo/-}$ KLRG1$^+$ effectors from donor K^b-OVA$^+$ CD8$^+$ T cells. (**E**) Donor CD45.2$^+$ central memory CD8$^+$ T cells were analyzed in the spleen 4 days after LM-OVA challenge. Representative dot plots with subset phenotypic analyses are shown; numbers represent percentages. (**F**) Representative histograms of stem cell–like and memory markers on total gated donor central memory CD8$^+$ T cells analyzed 4 days after LM-OVA challenge. (**G**) Total numbers of adoptively transferred donor central memory cells, before and after LM-OVA challenge. (**H**) Numbers of donor CD127$^+$ KLRG1$^-$ memory precursor and CD127$^{lo/-}$ KLRG1$^+$ effector CD8$^+$ T cells differentiated from donor central memory CD8$^+$ T cells. Graphs are representative of two experiments with three mice per group. All graphs show geometric means. *P < 0.05 (Wilcoxon Mann-Whitney test).

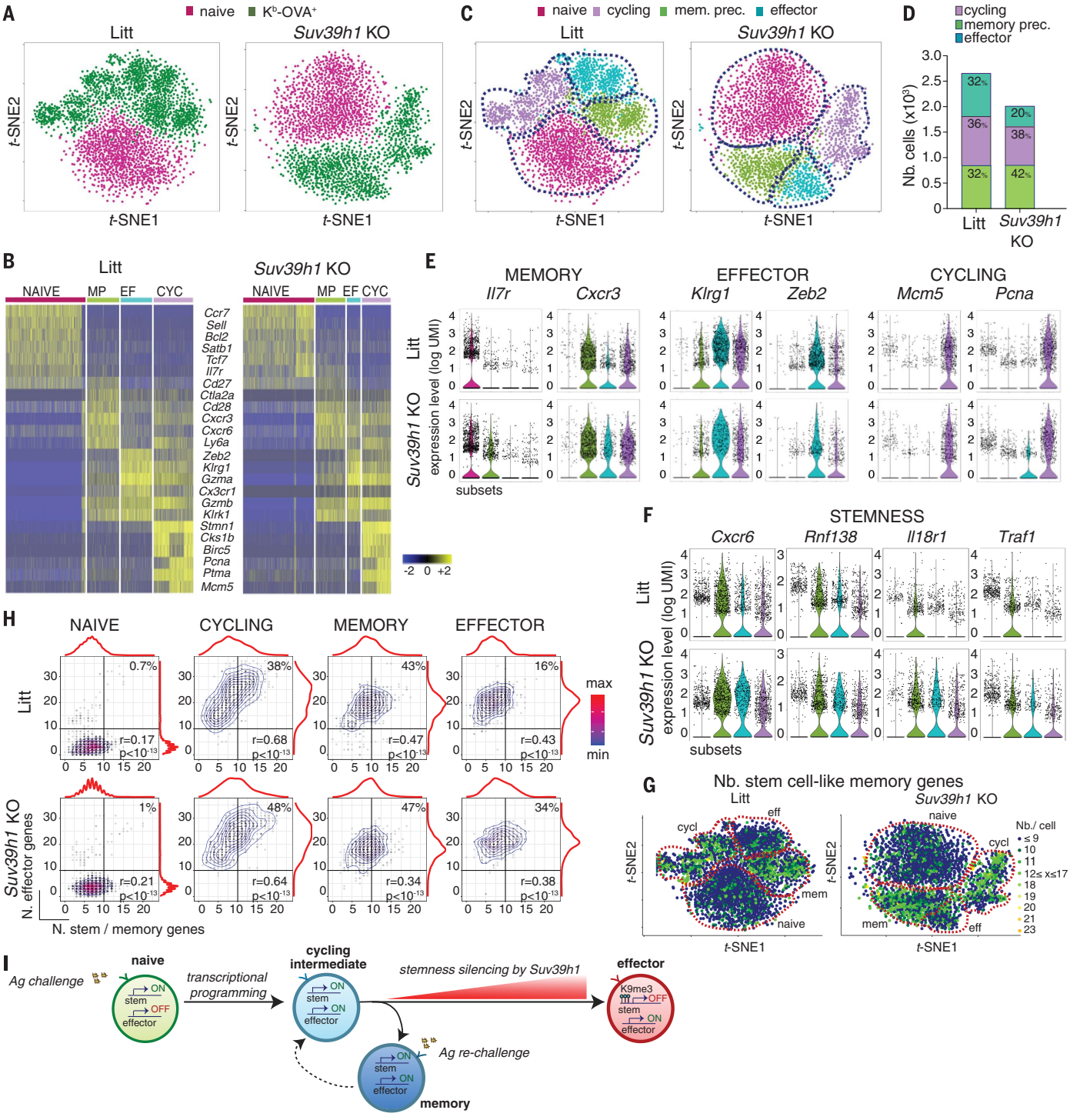

Fig. 6. Stem cell–like/memory genes are expressed by memory precursors and cycling CD8$^+$ T intermediates, and silenced by Suv39h1 in terminal effectors. (**A** to **H**) scRNA-seq analysis of naïve and K^b-OVA$^+$ CD8$^+$ T cells isolated from wild-type and *Suv39h1*-KO mice 7 days after LM-OVA infection. (A) Graph-based clustering by *t*-SNE projection of naïve and K^b-OVA$^+$ CD8$^+$ T cells isolated from wild-type and *Suv39h1*-KO mice. The colors indicate sorted CD8$^+$ T cell subsets. Each dot represents an individual cell. (B) Heat maps of six representative genes for each subset category identified. Columns represent cells; rows represent genes. The color scale is based on z-score distribution. (C) *t*-SNE projection of single cells, colored according to four major subset categories defined by semi-supervised clustering based on specific and distinct gene expression profiles. (D) Numbers and percentages of cells for each category. Violin plots in (E) and (F) show expression distribution of memory, effector, cycling, and stem cell/memory representative markers. (G) *t*-SNE projection of single cells, showing the number of stem cell–like memory genes expressed in each cell. (H) Density scatterplots represent numbers of effector versus stem cell/memory genes expressed in individual cells for each subset category. Color scale indicates gene density; marginal distributions show memory/stem (*x* axis) and effector (*y* axis) gene number distributions. Pearson linear regression is displayed for each plot. (**I**) Working model depicting the pivotal role of Suv39h1 during CD8$^+$ T cell lineage differentiation and commitment.

genes from both signatures. Thus, scRNA-seq analysis reveals the alternative expression of the stem/memory and effector signatures in the two cell types, respectively, and the concomitant low or high expression of these two signatures in the cycling cells. These results suggest that cycling cells may represent bipotent differentiation intermediates expressing both effector and stem/memory potential. Furthermore, the commitment to effector differentiation paths appears to be acquired by the silencing of stem/memory genes.

The total number of unique molecular identifiers (UMI) measured in each subset category did not differ between wild-type and *Suv39h1*-KO cells (fig. S17, A and B). Naïve, cycling, and memory *Suv39h1*-KO cells bear similar patterns of gene expression signatures as compared to wild-type cells. In contrast, a significant difference was observed in effector cells, in which the numbers of stem/memory genes per cell were increased relative to effector cells from wild-type mice. The proportion of cells expressing more than 10 genes from the stem/memory signature was augmented from 16% in the wild type to 34% in effector *Suv39h1*-KO cells. Thus, rather than a specific subpopulation of stem/memory cells accumulating in the *Suv39h1*-KO mice, the expression of stem/memory-related genes was derepressed mainly in *Suv39h1*-KO effector T cells.

Conclusions

We argue that after priming, cycling $CD8^+$ T lymphocytes reprogram both self-renewing and effector gene expression profiles (Fig. 6I). These cycling cells may represent bipotent intermediates, which would then repress either the effector or stem cell/memory programs while they differentiate to memory precursors or effectors, respectively (Fig. 6I). The silencing of the stem cell/memory gene expression program is under the control of Suv39h1 by imposing the H3K9me3 modification on chromatin at the corresponding loci. In doing so, Suv39h1/H3K9me3 would establish an epigenetic barrier on the stem/memory gene expression program, preventing effector reprograming into memory cells (Fig. 6I). It is most likely that the possibly reversible silencing of effector gene expression in memory cells occurs through other mechanisms, as memory cells do effectively reprogram into effectors upon rechallenge. These results open new perspectives for the manipulation of epigenetic programming of T lymphocyte identity in the context of vaccination, checkpoint-based immunotherapies, and adoptive T cell therapies.

REFERENCES AND NOTES

1. A. O. Kamphorst, K. Araki, R. Ahmed, *Vaccine* **33** (suppl. 2), B21–B28 (2015).
2. M. J. Bevan, *Nat. Immunol.* **12**, 463–465 (2011).
3. R. Ahmed, M. J. Bevan, S. L. Reiner, D. T. Fearon, *Nat. Rev. Immunol.* **9**, 662–668 (2009).
4. J. T. Chang, E. J. Wherry, A. W. Goldrath, *Nat. Immunol.* **15**, 1104–1115 (2014).
5. S. M. Kaech, W. Cui, *Nat. Rev. Immunol.* **12**, 749–761 (2012).
6. H. Y. Shih *et al.*, *Immunol. Rev.* **261**, 23–49 (2014).
7. N. P. Weng, Y. Araki, K. Subedi, *Nat. Rev. Immunol.* **12**, 306–315 (2012).
8. C. Maison, J. P. Quivy, A. V. Probst, G. Almouzni, *Cold Spring Harb. Symp. Quant. Biol.* **75**, 155–165 (2010).
9. G. Almouzni, A. V. Probst, *Nucleus* **2**, 332–338 (2011).
10. B. D. Fodor, N. Shukeir, G. Reuter, T. Jenuwein, *Annu. Rev. Cell Dev. Biol.* **26**, 471–501 (2010).
11. C. D. Allis, T. Jenuwein, *Nat. Rev. Genet.* **17**, 487–500 (2016).
12. C. Maison, G. Almouzni, *Nat. Rev. Mol. Cell Biol.* **5**, 296–304 (2004).
13. A. H. Peters *et al.*, *Cell* **107**, 323–337 (2001).
14. A. V. Probst, E. Dunleavy, G. Almouzni, *Nat. Rev. Mol. Cell Biol.* **10**, 192–206 (2009).
15. T. T. Onder *et al.*, *Nature* **483**, 598–602 (2012).
16. S. P. Bradley, D. A. Kaminski, A. H. Peters, T. Jenuwein, J. Stavnezer, *J. Immunol.* **177**, 1179–1188 (2006).
17. R. S. Allan *et al.*, *Nature* **487**, 249–253 (2012).
18. E. G. Pamer, *Nat. Rev. Immunol.* **4**, 812–823 (2004).
19. E. J. Wherry *et al.*, *Immunity* **27**, 670–684 (2007).
20. I. Hoebeke *et al.*, *Leukemia* **21**, 311–319 (2007).
21. C. J. Luckey *et al.*, *Proc. Natl. Acad. Sci. U.S.A.* **103**, 3304–3309 (2006).
22. L. Gattinoni *et al.*, *Nat. Med.* **17**, 1290–1297 (2011).
23. L. Spinelli, S. Carpentier, F. Montañana Sanchis, M. Dalod, T. P. Vu Manh, *BMC Genomics* **16**, 814 (2015).
24. B. Yu *et al.*, *Nat. Immunol.* **18**, 573–582 (2017).
25. G. Wei *et al.*, *Immunity* **30**, 155–167 (2009).
26. M. L. Miller *et al.*, *Proc. Natl. Acad. Sci. U.S.A.* **111**, 7397–7402 (2014).
27. F. Sallusto, D. Lenig, R. Förster, M. Lipp, A. Lanzavecchia, *Nature* **401**, 708–712 (1999).
28. P. Graef *et al.*, *Immunity* **41**, 116–126 (2014).
29. S. M. Kaech *et al.*, *Nat. Immunol.* **4**, 1191–1198 (2003).

ACKNOWLEDGMENTS

We thank all the U932 and UMR3664 members; C. Maison, N. Lacoste, and F. X. Gobert for helpful discussions; A. Cros and V. Mondin for technical help; B. Amati and J. Sedat for critical reading of the manuscript; the flow cytometry platform, the genomic and animal facilities, the Nikon Imaging Center of Curie Institute; and the PICT-IBISA@Pasteur Imaging facility. We thank T. Jenuwein for providing the *SUV39H1* gene and the *Suv39h1*-KO mice. LM-OVA was kindly provided by H. Shen. Supported by the Institute Curie, Institut National de la Santé et de la Recherche Médicale, Centre National de la Recherche Scientifique, ANR "ChromaTin" grant ANR-10-BLAN-1326-03, and "EPICURE" grant ANR-14-CE16-0009 (S.A. and G.A.); la Ligue Contre le Cancer (Equipe labelisée Ligue, EL2014.LNCC/SA) and Association de Recherche Contre le Cancer grant ERC (2013-AdG N° 340046 DCBIOX) (S.A.); la Ligue Nationale contre le Cancer (Equipe labelisée Ligue), the European Commission Network of Excellence EpiGeneSys (HEALTH-F4-2010-257082), ERC Advanced Grant 2009-AdG_20090506 "Eccentric," the European Commission large-scale integrating project FP7_HEALTH-2010-259743 "MODHEP," ANR-11-LABX-0044_DEEP, ANR-10-IDEX-0001-02 PSL, ANR "CHAPINHIB" ANR-12-BSV5-0022-02, ANR "CELLECTCHIP" ANR-14-CE10-0013, and the Aviesan-ITMO cancer project "Epigenomics of breast cancer" (G.A.); and SiRIC/INCa grant INCa-DGOS-4654 (J.J.W.). High-throughput sequencing was performed by the ICGex NGS platform of the Institut Curie supported by the grants SESAME (région Ile-de-France), ANR-10-EQPX-03, and ANR-10-INBS-09-08. The bioinformatics data are available in the Gene Expression Omnibus (GEO) database under accession numbers GSE105163 (microarrays) and SuperSeries GSE106268 for ChIP-seq and scRNA-seq data (linked to subseries GSE106264, GSE106265, and GSE106267). The authors have no conflicting financial interests. The data are tabulated in the main paper and in the supplementary materials. Author contributions: L.P. conceived and designed the project, carried out experimental work, and wrote the manuscript; C.G. contributed to bioinformatics design, carried out bioinformatics work, and interpreted data; E.Z. contributed to project design, carried out experimental work, and interpreted data; P.G. carried out bioinformatics work and participated in data interpretation; N.B. carried out experimental work; J.J.W. participated in bioinformatics data analysis and interpretation; J.-P.Q. participated in project design and data interpretation and wrote the manuscript; G.A. designed the project and wrote the manuscript; and S.A. conceived and designed the project and wrote the manuscript. L.P., C.G., and S.A. are inventors on patent application EP17305757.1 submitted by Institut Curie that covers the targeting of Suv39h1 in the context of T cell adoptive transfer.

SUPPLEMENTARY MATERIALS

www.sciencemag.org/content/359/6372/177/suppl/DC1
Materials and Methods
Figs. S1 to S17
Tables S1 to S5
References (*30*–*42*)

27 July 2016; resubmitted 1 August 2017
Accepted 16 November 2017
10.1126/science.aah6499

Science

The epigenetic control of stemness in CD8$^+$ T cell fate commitment

Luigia Pace, Christel Goudot, Elina Zueva, Paul Gueguen, Nina Burgdorf, Joshua J. Waterfall, Jean-Pierre Quivy, Geneviève Almouzni and Sebastian Amigorena

Science **359** (6372), 177-186.
DOI: 10.1126/science.aah6499

Epigenetic modulation of effector T cells

The epigenetic states and associated chromatin dynamics underlying the initiation and maintenance of memory and effector CD8$^+$ T cells are poorly understood. Pace *et al.* found that mice lacking the histone H3 lysine 9 methyltransferase Suv39h1 had markedly reduced antigen-specific effector CD8$^+$ T cell responses to *Listeria monocytogenes* infection (see the Perspective by Henning *et al.*). Instead, CD8$^+$ T cells in these mice were enriched for genes associated with naïve and memory signatures and showed enhanced memory potential and increased survival capacity. Thus, Suv39h1 marks chromatin through H3K9me3 deposition and silences memory and stem cell programs during the terminal differentiation of effector CD8$^+$ T cells.

Science, this issue p. 177; see also p. 163